JOURNAL OF GEOPHYSICAL RESEARCH, VOL. 108, NO. D11, 4341, doi:10.1029/2003JD003377, 2003

Sensitivity studies of the effect of increased aerosol concentrations and snow crystal shape on the snowfall rate in the Arctic

U. Lohmann and J. Zhang

Department of Physics and Atmospheric Science, Dalhousie University, Halifax, Nova Scotia, Canada

J. Pi

Computer Science Department, University of Nebraska at Omaha, Omaha, Nebraska, USA

Received 5 January 2003; accepted 28 February 2003; published 7 June 2003.

[1] The mesoscale model GESIMA is used to simulate microphysical properties of Arctic clouds and their effect on radiation. Different case studies during the FIRE ACE/SHEBA project show that GESIMA is able to simulate the cloud boundaries, ice and liquid water content, and effective radii in good agreement with observations. For two different aerosol scenarios, the simulation results show that the anthropogenic aerosol can alter microphysical properties of Arctic clouds, and consequently modify surface precipitation. *Borys et al.* [2000] proposed that anthropogenically induced decreases in cloud droplet size inhibit the riming process. On the contrary, we find that the accretion of snow crystals with cloud droplets is increased in the polluted cloud owing to its higher cloud droplet number concentration. Instead, the autoconversion rate of cloud droplets and accretion of drizzle by snow decreases caused by the shutdown of the collision-coalescence process in the polluted cloud. The amount of precipitation reaching the surface as snow depends crucially on the crystal shape. If aggregates are assumed, then a tenfold increase in aerosol concentration leads to an increase in accumulated snow by 40% after 7 hours of simulation whereas the snow amount decreases by 30% when planar crystals are assumed because of the larger accretion efficiency of snow crystals with cloud droplets in case of aggregates. *INDEX TERMS:* 0305 Atmospheric Composition and Structure: Aerosols and particles (0345, 4801); 0320 Atmospheric Composition and Structure: Cloud physics and chemistry; 0345 Atmospheric Composition and Structure: Pollution—urban and regional (0305); 3349 Meteorology and Atmospheric Dynamics: Polar meteorology; 3354 Meteorology and Atmospheric Dynamics: Precipitation (1854); *KEYWORDS:* arctic haze, snowfall rate, aerosols, mesoscale cloud modeling

Citation: Lohmann, U., J. Zhang, and J. Pi, Sensitivity studies of the effect of increased aerosol concentrations and snow crystal shape on the snowfall rate in the Arctic, *J. Geophys. Res.*, *108*(D11), 4341, doi:10.1029/2003JD003377, 2003.

1. Introduction

[2] Recent climate modeling results highlighted the Arctic as a region of particular importance and vulnerability to global climate change [*Houghton et al.*, 2001]. A dominant feature of the Arctic is the presence of temperature and humidity inversions, particularly during the coldest half of the year. The temperature inversions are caused by radiative cooling, warm air advection, subsidence, cloud processes, surface melt, and topography [*Curry*, 1983]. Ice crystal precipitation in the lower layers depletes the moisture in those layers which accounts for the moisture inversions.

[3] Climatologies of cloud fraction over the Arctic are primarily derived from surface observations [*Huschke*, 1969; *Gorshkov*, 1983]. These climatologies show broad agreement, with a maximum total cloud cover as high as 90% during summer and a minimum during winter (40%–68%). Global satellite cloud climatologies have also provided analyses for the Arctic. Comparison of the ISCCP satellite cloud analyses with surface observations [*Schweiger and Key*, 1992], however, showed that the monthly averaged ISCCP cloud amounts are generally 5%–35% less than the surface based climatology described by *Warren and Wiscombe* [1980].

[4] So far, Arctic climate modeling has been conducted mainly with general circulation models (GCMs), but physical parameterizations in GCMs related to clouds and radiation are incapable of capturing key futures of the Arctic [*Curry et al.*, 1996]. *Lohmann et al.* [2001] used the single-column model (SCM) of the Canadian GCM to simulate the evolution of ice clouds for three different flights during the First ISCCP Regional Experiment Arctic Cloud Experiment (FIRE ACE) in April 1998. The SCM in its original setup overpredicts the ice crystal concentrations measured with the 2DC probe but the agreement with observations improved when an empirical

0148-0227/03/2003JD003377$09.00

linear relationship between the aerosol and ice crystal number deduced from FIRE ACE was applied. *Zhang and Lohmann* [2003] compared different cloud schemes during Arctic spring and found that statistical cloud schemes that simultaneously predict cloud cover and cloud condensate are superior to explicit cloud schemes, which prognose cloud condensate but empirically obtain cloud cover from either relative humidity only or from relative humidity and cloud condensate.

[5] Cloud resolving models (CRMs), on the other hand, have much higher spatial and temporal resolutions, and thus GCM subgrid-scale variability of clouds can be resolved in CRMs. This seems to be crucial for Arctic cloud simulations. Only a few Arctic cloud simulations have been conducted with CRMs. *Jiang et al.* [2000] used a two-dimensional CRM to simulate mixed-phase Arctic stratus. They conducted experiments of the model's sensitivity to the concentration of ice forming nuclei and large-scale advection. They found that midlatitude parameterizations did not work well in the Arctic. Only when they decreased the number of ice forming nuclei to 30% of the values given for midlatitudes by *Meyers et al.* [1992] and increased the horizontal advection rates from NCEP reanalysis by a factor of 3, then the mixed-phase stratus was maintained and its water content agreed well with observations. *Girard and Blanchet* [2001] have applied an explicit aerosol-cloud-radiation model to simulate Arctic diamond dust, ice fog, and thin stratus. They are able to simulate cloud phase, particle size, ice crystal number, and mass concentration in agreement with observations.

[6] If the droplet size decreases below 10 μm in diameter, the riming efficiency (the collection of supercooled cloud droplets by falling ice crystals) rapidly approaches zero for all snow crystal sizes [*Pruppacher and Klett*, 1997]. Therefore *Borys et al.* [2000] hypothesized from analyzing wintertime frontal systems and orographic snowfall events in northwest Colorado that anthropogenically induced decreases in cloud droplet size may affect precipitation in cold clouds through inhibition of the riming process. Pollution peaks of anthropogenic aerosols and their precursors associated with long range transport from Eurasia are not uncommon in the Arctic [*Barrie*, 1996]. Therefore we will investigate in this paper what influence anthropogenic aerosols may have on precipitation in the Arctic.

[7] The mesoscale model GESIMA and its cloud parameterization scheme are described in section 2. This study will use GESIMA to simulate clouds for specific cases during the FIRE ACE campaign as outlined in section 3. Section 4 presents simulation results with GESIMA for two specific cases during the FIRE ACE campaign. The modeling results are compared with observational data measured by aircraft-based instruments, radar, lidar, microwave radiometer and rain gauges. In section 5, two aerosol scenarios and two different snow crystal habits are assumed in order to study the aerosol effect on microphysical processes and surface precipitation. The conclusions are given in section 6.

2. Model Description

[8] In this study the three-dimensional, time-dependent, nonhydrostatic mesoscale model GESIMA [*Kapitza and Eppel*, 1992] is used with a cloud scheme developed for numerical studies of cirrus and stratus clouds and verified with observations as described by *Levkov et al.* [1992]. Predicted variables are the three velocity components, the potential temperature, the mixing ratio of water vapor and the mixing ratios and number concentrations of the cloud species (cloud droplets, ice crystals, rain and snow). The system of the atmospheric equations in the dynamical part of GESIMA is based on the conservation laws for momentum, energy, and mass. The momentum equations and the equation for the potential temperature are integrated in time by a predictor-corrector scheme, while all water species are integrated with a simple forward scheme every 10 seconds for a total simulation time of 7 hours. The eddy diffusion terms are calculated by a first order closure according to the level 2.5 scheme in the hierarchy of *Mellor and Yamada* [1974]. The radiation scheme is called every 10 minutes.

[9] The mesoscale model uses 25 × 25 grid points horizontally to provide a 2 km horizontal resolution over a 50 km × 50 km region where the ice breaker ship was located during the FIRE ACE/SHEBA campaign (as described in Section 3). The vertical domain is 9 km with variable resolution ranging from about 50 m near the surface to 300 m near 9 km using a total of 46 vertical levels.

[10] Parameterized microphysical processes are condensational growth of cloud droplets, depositional growth of ice crystals, homogeneous, heterogeneous and contact freezing of cloud droplets, autoconversion of cloud droplets, aggregation of ice crystals, accretion of ice crystals, cloud droplets and drizzle by snow, accretion of cloud droplets by rain, evaporation of cloud liquid water and rain, sublimation of ice crystals and snow, melting of ice crystals and snow and sedimentation of ice crystals, snow flakes and raindrops.

[11] We replaced the autoconversion rate of cloud droplets to form rain drops and the accretion rate of cloud droplets by raindrops by *Berry and Reinhardt* [1973] with the parameterization developed by *Khairoutdinov and Kogan* [2000] because the dependence of the autoconversion rate on liquid water content in the *Khairoutdinov and Kogan* [2000] scheme is in better agreement with solutions of the stochastic collection equation using different observed cloud droplet distributions [*Wood*, 2002]. We also introduced the parameterization of cloud droplet nucleation by *Ghan et al.* [1993] where the number of nucleated cloud droplets N_c is a function of the vertical velocity w and the accumulation mode aerosol number concentration N_a:

$$N_c = \frac{wN_a}{w + cN_a} \tag{1}$$

where N_a is in cm^{-3}, w in cm s^{-1} and $c = 0.0034$ cm^4 s^{-1}, valid for ammonium sulfate, assuming a lognormal size distribution with a mode radius of 0.05 μm and geometric width $\sigma = 2$ at 800 hPa and 273 K.

[12] The parameterizations of a variety of accretional growth mechanisms involved in the model are mainly based on the approach described by *Lin et al.* [1983]. In the model, riming (the snow crystals settling through a population of supercooled cloud droplets, colliding and coalescing with them) takes place when the cloud water content q_W exceeds 10^{-5} kg kg^{-1}. The rate of change in snow mixing ratio q_S due to riming is based on the geometric sweep-out

integrated over all snow sizes with an assumed exponential snow size distribution:

$$\left(\frac{\partial q_S}{\partial t}\right)_{riming} = \frac{\pi E_{SW} n_{0S} a q_W \Gamma(3+b)}{4\lambda_S^{(3+b)}} \left(\frac{\rho_0}{\rho}\right)^{0.5} \quad (2)$$

where $n_{0S} = 3 \times 10^6$ m^{-4} is the intercept parameter, λ_S is the slope of the exponential Marshall-Palmer snow crystal size distribution, $a = 4.84$, $b = 0.25$, ρ is the air density and $\rho_0 = 1.3$ kg m^{-3} is a reference density. The collection efficiency E_{SW} is highly dependent on the cloud droplet and snow crystal size [*Pruppacher and Klett*, 1997]. Here we introduce the size dependent collection efficiency for planar ice crystals as suggested by *Mitchell* [1990] and for aggregates as measured by *Lew et al.* [1986] instead of the constant value of 1 that GESIMA previously assumed. The maximum dimensions of a planar crystal d_{pl} (m) and aggregate d_{agg} (m), that are needed to calculate the fall speed and the Stokes number for the accretion efficiency, are obtained from empirical mass-maximum dimension relationships and the snow crystal number concentration N_S (m^{-3}) as described by *Rogers and Yau* [1989] and *Pruppacher and Klett* [1997], respectively:

$$d_{pl} = 10^{-2} \sqrt{\frac{q_S \cdot 10^3 \rho}{3.8 \cdot 10^{-4} N_S}} \quad (3)$$

$$d_{agg} = 10^{-3} \left(\frac{q_S \cdot 10^6 \rho}{0.04 N_S}\right)^{0.714} \quad (4)$$

In case of planar crystals, the empirical fall speed formulae from *Rogers and Yau* [1989] $u = 2.34\ (100\ d_{pl})^{0.3}$ is used where u is the snow crystal fall speed in m/s. We assume that aggregates can be approximated by equivalent spheres as assumed in the standard GESIMA configuration [*Levkov et al.*, 1992].

[13] E_{SW} is shown as a function of snow crystal diameter and cloud droplet diameter for planar crystals in Figure 1. The expression for aggregates is only valid for a limited range at Reynolds numbers above 40 and Stokes numbers between 0.06 and 0.3 (not shown). Outside this range, we use the accretion efficiency of planar crystals. The discontinuities of E_{SW} in Figure 1 stem from the empirical data that are used by *Mitchell* [1990] to derive the collection efficiency as a function of the Reynolds and Stokes number of the flow. The major difference in the collection efficiency between planar crystals and aggregates arises because for the same snow water content and snow crystal number concentration planar crystals are about one order of magnitude larger and thus have a smaller collection efficiency than aggregates (see Figure 1 and equations (3) and (4)).

3. Data Description

[14] The FIRE (First ISCCP (International Satellite Cloud Climatology Project) Regional Experiment) ACE (Arctic Clouds Experiment) was conducted during April–July, 1998 to study Arctic cloud systems under spring and summer conditions [*Curry et al.*, 2000; *Korolev et al.*, 1999]. The scientific objectives of FIRE ACE are to study the impact of Arctic clouds on the radiation exchange between surface, atmosphere and space, and the influence of surface characteristics on these clouds. The FIRE ACE data set is well suited to focus on improving current climate model simulations of the Arctic climate, especially with respect to clouds and their effects on the surface energy budget, cloud microphysics and atmospheric chemistry.

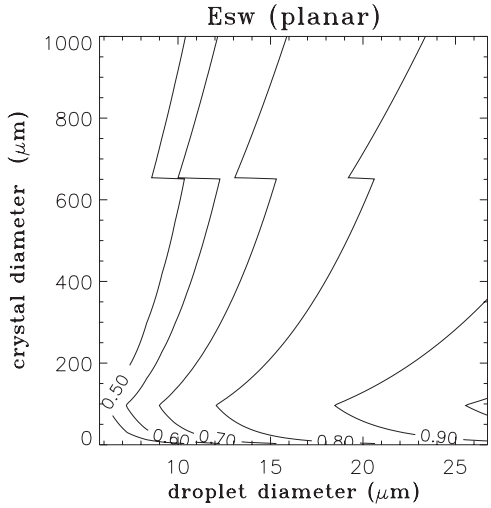

Figure 1. Collection efficiency of snow flakes with cloud droplets as a function of crystal and droplet size and for planar crystals.

[15] The strategy of FIRE ACE was to use aircrafts to take remote and in-situ measurements of Arctic clouds and surface characteristics. The FIRE ACE project was collocated with the SHEBA (Surface Heat Budget of the Arctic Ocean) project [*Uttal et al.*, 2002]. SHEBA is a research program designed to document and understand the physical processes that couple the atmosphere, ice and ocean in the Arctic. It was a yearlong extensive set of measurements directly on, under and above the sea ice in the Beaufort sea, using the Canadian Coast Guard ice breaker Des Groseilliers as a permanent ice station. A number of key surface-based remote sensing instruments specially designed for the measurements of clouds and radiation were deployed at the SHEBA ice station.

[16] Temperature, pressure and surface precipitation were obtained from an integrated SHEBA data set at University of Washington. Precipitation was measured by a weighing gauge. The initial data required by GESIMA are potential temperature, wind speed, relative humidity and aerosol number concentration. Besides aerosol number concentration which was measured by a Condensation Particle Counter (CPC-7610) mounted on the Canadian Convair-580 aircraft, other initial variables were obtained from rawinsonde data. Due to rawinsonde sensor contamination the original relative humidity data are too dry. Here the corrected relative humidity data provided by Dr. Moritz (personal communication) were used.

[17] The Canadian Convair-580 sampled clouds over the SHEBA ship in April, 1998. It was extensively equipped for cloud microphysical measurements [*Korolev et al.*, 1999]. The Canadian aircraft operated out of Inuvik, Northwest

Territories, and Barrow, Alaska. The Nevzorov liquid water probe was used to measure liquid water content (LWC) and Total Water Content (TWC) in the particle size range from 5 μm to approximately 1000 μm. Theoretically, the ice water content (IWC) can be obtained by subtracting LWC from TWC, but the Nevzorov LWC probe also responds to IWC in a mixed phase cloud, with an average response of approximately 15–20% [*Cober et al.*, 2001]. The accuracy of the Nevrozov LWC probe is 0.003–0.005 g m^{-3} while the error of the TWC probe can be as high as 0.02 g m^{-3}. This can introduce large errors in the computation of LWC and IWC. To minimize the problem, we used 10 s averaged data rather than 1 s averages.

[18] LWC and IWC can be derived from the measured LWC (LWC_{mea}) and TWC (TWC_{mea}) following *Cober et al.* [2001] as follows:

$$IWC = 1.25 \cdot (TWC_{mea} - LWC_{mea}) \tag{5}$$

$$LWC = TWC_{mea} - IWC \tag{6}$$

[19] The lidar on the SHEBA ship is a Depolarization and Backscatter-Unattended Lidar (DABUL). It is a pulsed laser-radar system operating at 523 nm wavelength [*Uttal et al.*, 2002]. The vertical resolution is 30 meters, and the time resolution is 5 seconds. A Millimeter Cloud Radar (MMCR) was deployed on the SHEBA ship. MMCR is a 35 GHz cloud profiling radar designed by the Environmental Technology Laboratory for unattended, long-term cloud monitoring [*Shupe et al.*, 2001]. It is a vertically pointing, low-peak-power and pulsed Doppler system. Its data are available every minute.

[20] IWC [g m^{-3}] and ice crystal effective radius (ratio of the third moment over the second moment of the cloud droplet size distribution) were also retrieved from radar [*Shupe et al.*, 2001]:

$$IWC = aZ^b \tag{7}$$

$$r_e = 0.14\left(\frac{Z}{74 \times 10^{-6} IWC}\right)^{\frac{1}{1.9}} \tag{8}$$

Here r_e is the ice crystal effective radius, Z is radar reflectivity, $a = 0.1$ and $b = 0.65$. Retrievals of effective radius may be biased toward larger ice particle sizes because the radar backscatter is proportional to the 6th moment of the size distribution. Based on the observed radar reflectivity and optical thickness inferred from IR radiometer measurement, the coefficients a and b are determined and the effective radius and ice water content are calculated. The errors of the fixed Z-IWC regressions can be as high as one order of magnitude, though typically they are about a factor of 2. Multiparameter retrievals provide a better accuracy of about 50–70% for IWC and 30–40% for the characteristic size [*Matrosov*, 1997].

[21] Cloud base and cloud top measured by lidar and radar were available every 10 minutes from the SHEBA data sets. We also used hourly mean microwave radiometer data of water vapor mass and liquid water path [*Lin et al.*, 2001].

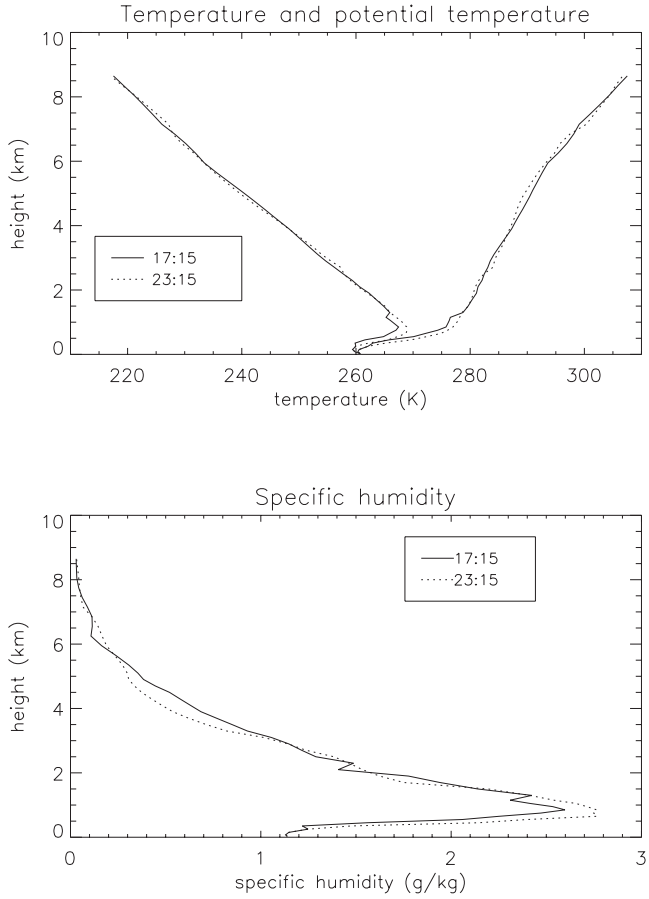

Figure 2. Vertical profiles of temperature, potential temperature, and specific humidity profiles based on the rawinsonde data taken at 1715 and 2315 UTC on 16 April 1998.

4. Comparison of GESIMA With Observations

4.1. The 16 April Case Study

[22] The first case study (flight 7 of the Canadian Convair-580) during FIRE ACE took place on 16 April 1998. A deep, single-layer precipitating mixed-phase cloud was observed on that day with a radar echo from the surface to 5 km and a strong temperature inversion at 1 km. The MMCR observed a mixed phase cloud between 1700–2400 UTC with a liquid water path of 20–40 g m^{-2}. The ice water path varied between 10 g m^{-2} and over 300 g m^{-2} during that time. The aircraft took off from Barrow at 2026 UTC and reached the SHEBA ship at 2207 UTC, where it descended from 7200 m down to 156 m within 40 minutes. It began the next ascend at 2249 UTC and reached the highest altitude at 2328 UTC. The model simulation is initialized with the rawinsonde taken at 1715 UTC as shown in Figure 2. It shows the temperature and moisture inversions in the boundary layer that increase with time.

[23] The simulated domain is initially horizontally homogeneous. A random temperature perturbation between 1200 m and 6000 m with a magnitude 0.1 K was applied for the first 10 minutes of the simulation. Based on the initial

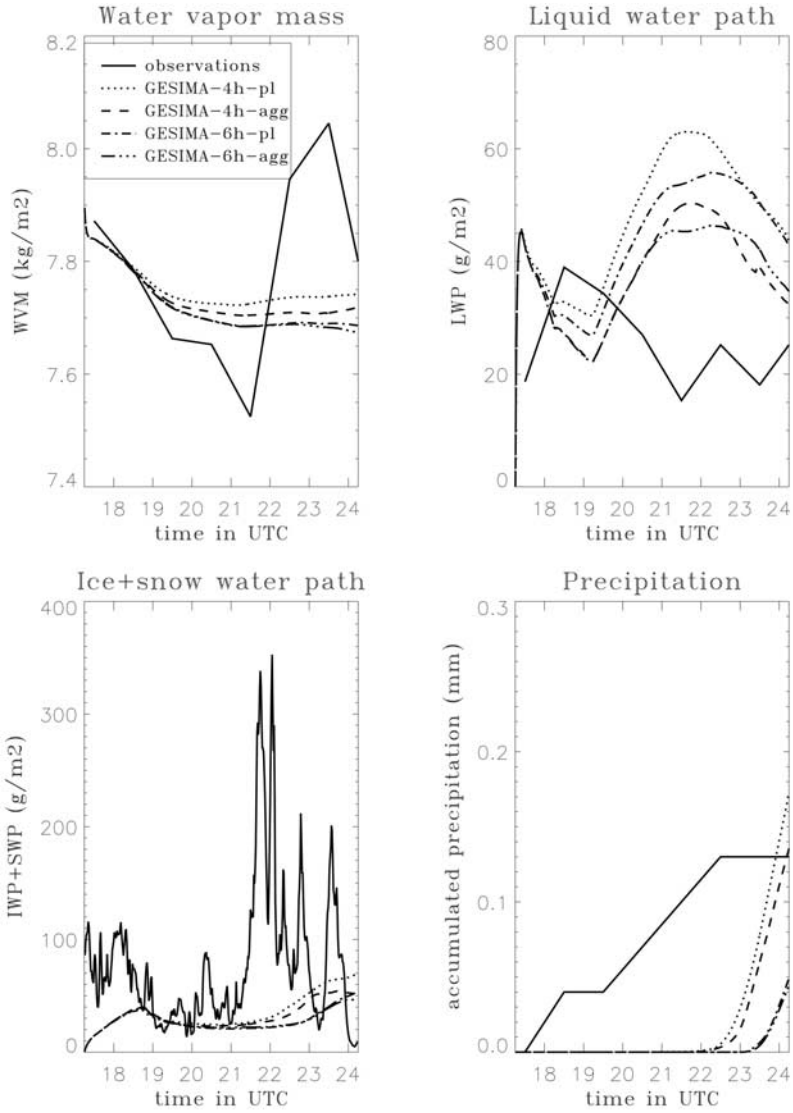

Figure 3. Temporal evolution of water vapor mass, liquid water path, ice and snow water path and precipitation from observations and 4 simulations with GESIMA using a 4-hour and 6-hour nudging time scale assuming planar crystals (pl) and aggregates (agg) on 16 April 1998.

profiles of potential temperature and specific humidity and those after 6 hours as shown in Figure 2, nudging of these simulated two variables to the observed values with different nudging timescales of 4 and 6 hours was applied. Nudging [*Lohmann et al.*, 1999] is a technique that relaxes the model state toward observational data by adding an additional term to the model equations:

$$\frac{\partial X}{\partial t} = Te_x + \frac{(X_{obs} - X_0)}{\tau_x} \tag{9}$$

where X presents the prognostic variable, Te_x is the tendency of the variable X as calculated by GESIMA, τ_x is the nudging time scale, and X_{obs} and X_0 are the observed and model calculated values of X.

[24] Figure 3 shows the temporal evolution of water vapor mass, liquid water path, the sum of ice and snow water path, and precipitation from observations and the GESIMA simulations using a 4-hour and 6-hour nudging timescale. For each nudging timescale two simulations that only differ in the snow crystal shape were conducted. We assume the crystals to be either planar crystals (GESIMA-4h-pl, GESIMA-6h-pl) or aggregates (GESIMA-4h-agg, GESIMA-6h-agg), respectively.

[25] The water vapor mass varies between 7.5 and 8.1 kg m^{-2}. GESIMA cannot capture these variations as the radiosonde profiles, to which GESIMA is nudged, are only available every 6 hours. Given that the water vapor mass is obtained from microwave radiometer measurements, the agreement is very good. After approximately one hour, the magnitude of liquid water path and ice water path is captured in all GESIMA simulations. After 2000 UTC, the agreement diverges as the observations predict more condensate to be in the solid phase whereas it remains in the liquid phase in GESIMA. The differences between the

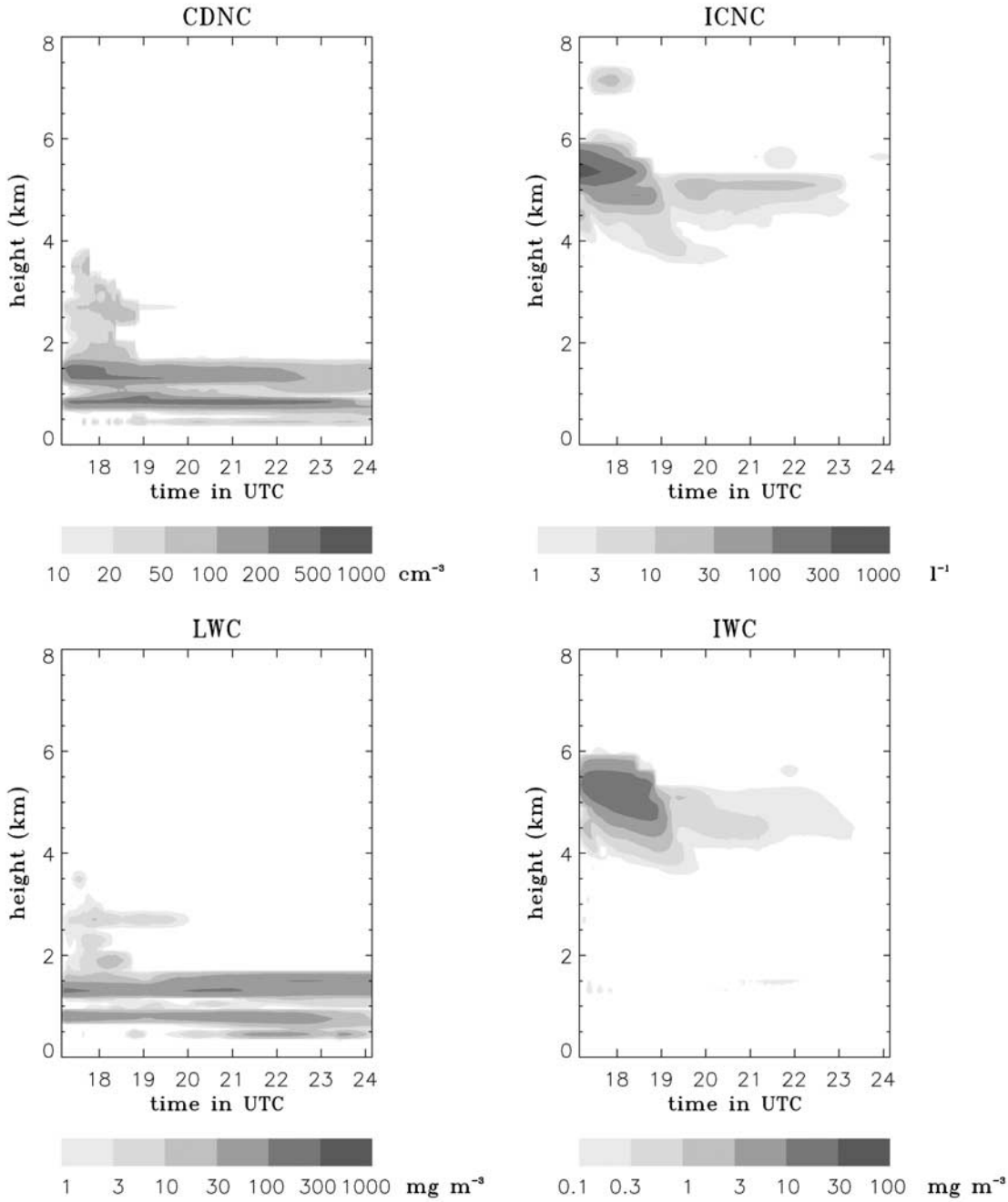

Figure 4. Temporal evolution of the simulated cloud droplet (CDNC), ice crystal (ICNC) number concentrations, liquid (LWC), and ice (IWC) water contents horizontally averaged over the cloudy part of the domain on 16 April 1998.

different simulations are smaller than the differences between GESIMA and the observations pointing to either systematic problems with the freezing parameterization in GESIMA or to problems of distinguishing liquid and ice clouds from observations or to problems with the forcing data [see also *Zhang and Lohmann*, 2003].

[26] The observed accumulated precipitation was calculated based on the hourly values of observational precipitation intensity measured from the SHEBA ship. The differences in nudging timescale appear to be most pronounced in the accumulated precipitation as only a fraction of the cloud condensate is converted to precipitation. Since cloud droplets and ice crystals cannot grow to precipitable size within the first hour, there is only slight precipitation during that period regardless of the nudging timescale. To take this into account, we start to accumulate the observed precipitation after 1815 UTC. The accumulated precipitation after 7 hours varies from 0.05 mm if a 6-hour nudging timescale is applied to 0.17 mm if a 4-hour nudging timescale is used and planar crystals are assumed. The difference is

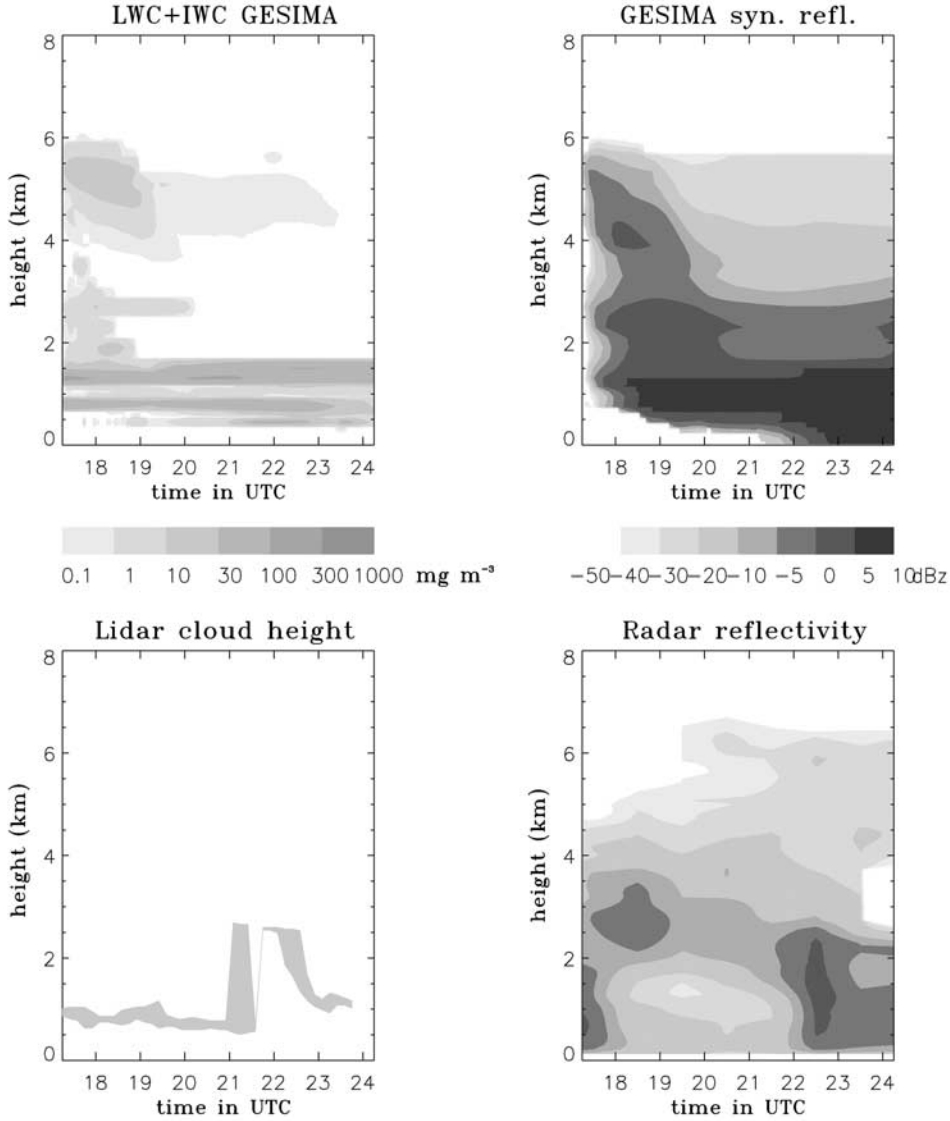

Figure 5. Temporal evolution of the domain averaged cloud altitude simulated by GESIMA as obtained from the sum of liquid and ice water content, synthetic reflectivity calculated from GESIMA, cloud base detected by lidar, and reflectivity obtained by the radar deployed on SHEBA ship on 16 April 1998.

reduced when snow crystals are assumed to be aggregates. As the simulation using a 4-hour nudging timescale assuming aggregates agrees best with the observed precipitation after 7 hours (0.136 mm versus 0.13 mm) and yet its ice and snow water path is not that much smaller than assuming planar crystals, we focus on the 4-hour nudging timescale simulations with aggregates for the remainder of this paper.

[27] Figure 4 shows that a liquid water cloud initially forms between 700 m and 4000 m. By 1900 UTC, the upper portion of the cloud is frozen and cloud top of the liquid cloud layer decreases down to 1700 m. The cloud becomes denser and cloud base starts to extend downward to 400 m by 1900 UTC. The increase in cloud liquid water is caused by the temperature inversion in the boundary layer that inhibits vertical mixing and thus leads to a buildup of water vapor evaporated from the surface. Two ice clouds form, an altostratus layer between 4 km and 6 km and a thin cirrus at 7 km. The altostratus cloud is initially characterized by high ice crystal number concentrations and ice water contents. As aggregation sets in and snow flakes form, the ice crystal number concentration and ice water content decrease. Also, the ice crystal number decreases toward cloud base as a result of aggregation as observed in nimbostratus [*Rogers and Yau*, 1989].

[28] Figure 5 shows the cloud thickness simulated by GESIMA and observed by lidar and radar. Since the emitted laser beam was attenuated quickly in the thick cloud, the lidar could not penetrate the whole cloud layer and only detects cloud base. The radar signal, on the other hand, is not attenuated and can detect the whole cloud. Since the radar is very sensitive to large particles, we compute the synthetic

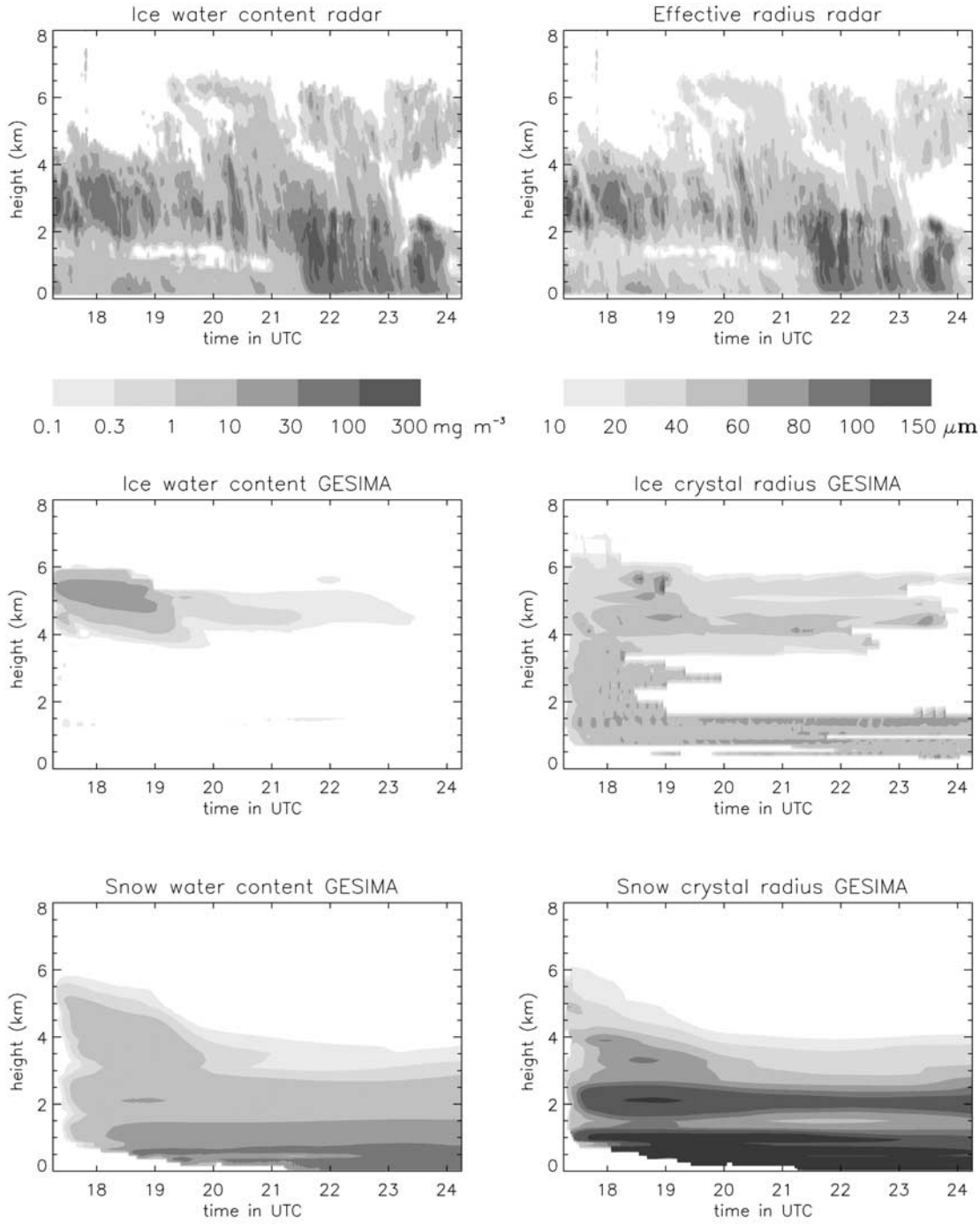

Figure 6. Temporal evolution of IWC and effective radius retrieved from radar and IWC and snow water content (SWC) and their effective radii simulated by GESIMA on 16 April 1998.

reflectivity calculated from the simulated liquid and ice water content, rain and snow flux and cloud droplet number concentration inverting the retrieval method used by *Shupe et al.* [2001] and to compare to the radar reflectivity. We take the sum of the liquid and ice water content for comparison with the lidar measurements. The cloud base agrees very well with lidar measurements prior to 2200 UTC after which the lidar measures a higher cloud base than simulated. On the other hand, the radar detects a signal down to the surface the whole time. In GESIMA it takes until 2115 UTC before the precipitation reaches the surface (see also Figure 3). The simulated radar echo top is around 6 km when deduced from calculations of synthetic reflectivity which corresponds to the averaged observed radar echo top (Figure 5).

[29] Figure 6 shows the detailed evolution of the ice water content and effective radius of the cloud as detected

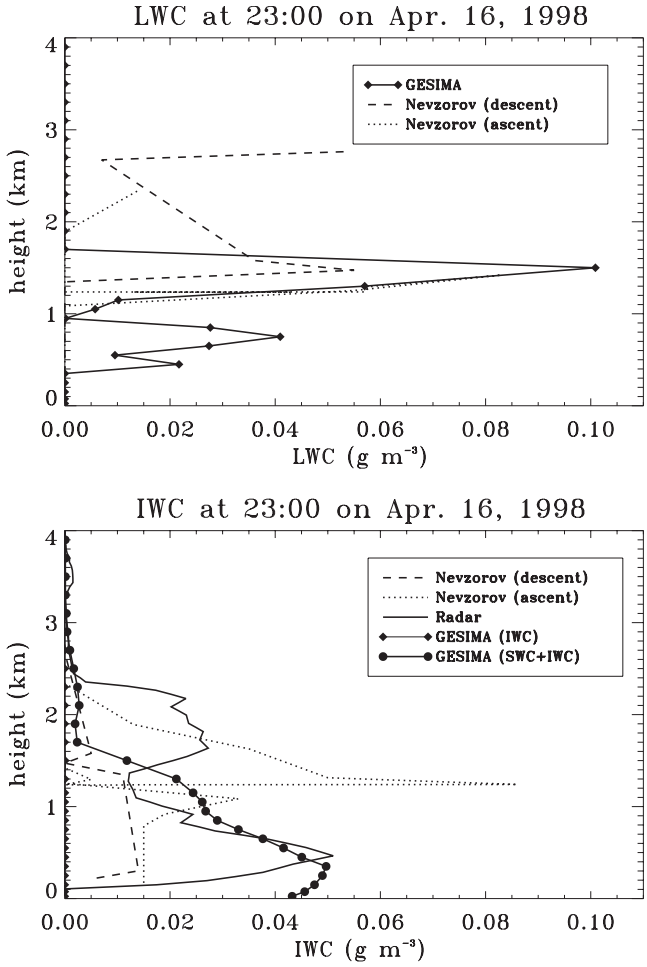

Figure 7. Vertical profiles of LWC and IWC at 2300 UTC on 16 April 1998 simulated by GESIMA and measured by aircraft and radar retrieval. The aircraft LWC and IWC were the derived ones according to equations (5) and (6) based on 10 s averaged data.

from radar. The observed maximum ice water content and effective radii occur initially between 2 and 4 km and extend to the surface after 2100 UTC. As the radar detects ice and snow crystals, we show ice water content and snow water content from GESIMA. In GESIMA, the ice water content occurs between 4 and 6 km and decreases with time as aggregation forms snow flakes. These snow flakes sediment and reach the surface by 2100 UTC. In agreement with observations, the largest water contents and the largest crystals are simulated in the lower layers but the snow water content is larger than observed below 1.5 km before 2130 UTC. The simulated effective ice crystal and snow crystal radii agree well with the radar retrieval with small ice and snow crystals at the top of the cloud and larger ones at the bottom. However, GESIMA overestimates the snow crystal size near the surface and underestimates the temporal variability of ice and snow water content and effective radii in and below the cloud. As shown in Figure 5, the overestimation of the snow water content in GESIMA in lower levels leads to a more pronounced overprediction of radar reflectivity. Apart from the initially high ice and snow water content between 4 and 6 km, the decrease of radar reflectivity with height is captured.

[30] Figure 7 shows the comparison of the simulated and measured liquid and ice water content from the Canadian aircraft and the radar. From the aircraft measurements of condensed water content, we can infer that the mixed-phase cloud exists mainly between 1000 and 2600 m. The cloud water content derived from the radar in a mixed phase cloud assumes that the radar signal is dominated by ice crystals. Therefore only ice water content is retrieved which may be a source of error. Also, the radar data has a cutoff of 0.005 g m^{-3} for cloud water content suggesting that the real cloud may occur over a deeper range than can be obtained from the radar retrieval. The simulated liquid water cloud is lower than observed with one maximum between 1 and 2 km and two secondary peaks below 1 km. Its maximum liquid water content exceeds the observed value derived from microphysics measurements during ascent by 0.02 g m^{-3} and by 0.04 g m^{-3} during descent. However, one has to keep in mind that the discrepancy with the ascending aircraft measurements is only as large as the error for the derived liquid and ice water content from the aircraft data using equations (5) and (6) of 0.02 g m^{-3} and thus falls in the measured uncertainty. The simulated sum of snow and ice water content below 3 km falls in between the microphysics measurements during ascent and descent and the value retrieved by the radar. In summary, GESIMA essentially captures the features of the observed cloud on 16 April 1998.

4.2. The 28/29 April Case Study

[31] This case study uses data from flight 17 of the Canadian Convair-580 on 28/29 April 1998. A midlevel ice cloud forms at 1400 on 28 April with cloud base at 4 km and cloud top between 6–8 km. The cloud deepens until 2400 with the cloud base lowering to 2.5 km based on the radar and lidar observations. Thereafter the cloud top decreased and the cloud thinned until 0300 UTC on 29 April (Figure 8) after which a generating cell appeared at 7.5 km. However, its ice water content increased so that the lidar could not penetrate the cloud any longer. At 0400 UTC the cloud broke up into two layers. The ice water content of the upper cirrus cloud increased due to the generating cell aloft whereas the lower cloud slowly sublimated (Figure 9). The surface temperature is −19.5°C. The aircraft flew from Barrow at 2207 UTC and reached the SHEBA ship at 2350 UTC, where it descended and reached the lowest altitude at 0030 UTC on 29 April 1998. Then it ascended and reached the highest altitude at 0116 UTC. The model is initialized with corrected rawinsonde data taken at 2315 UTC on 28 April 1998 and the total simulation time is 7 hours. A random temperature perturbation between 2 km and 8 km with a magnitude 0.1 K was applied for the first 10 minutes of the simulation. As this case has pure ice clouds and is non precipitating, there is hardly any difference between assuming aggregates or planar crystals and we focus again on the 4-hour nudging timescale simulation with aggregates.

[32] As shown in Figure 8, GESIMA simulates cloud base at 2.5 km as detected from both lidar and radar.

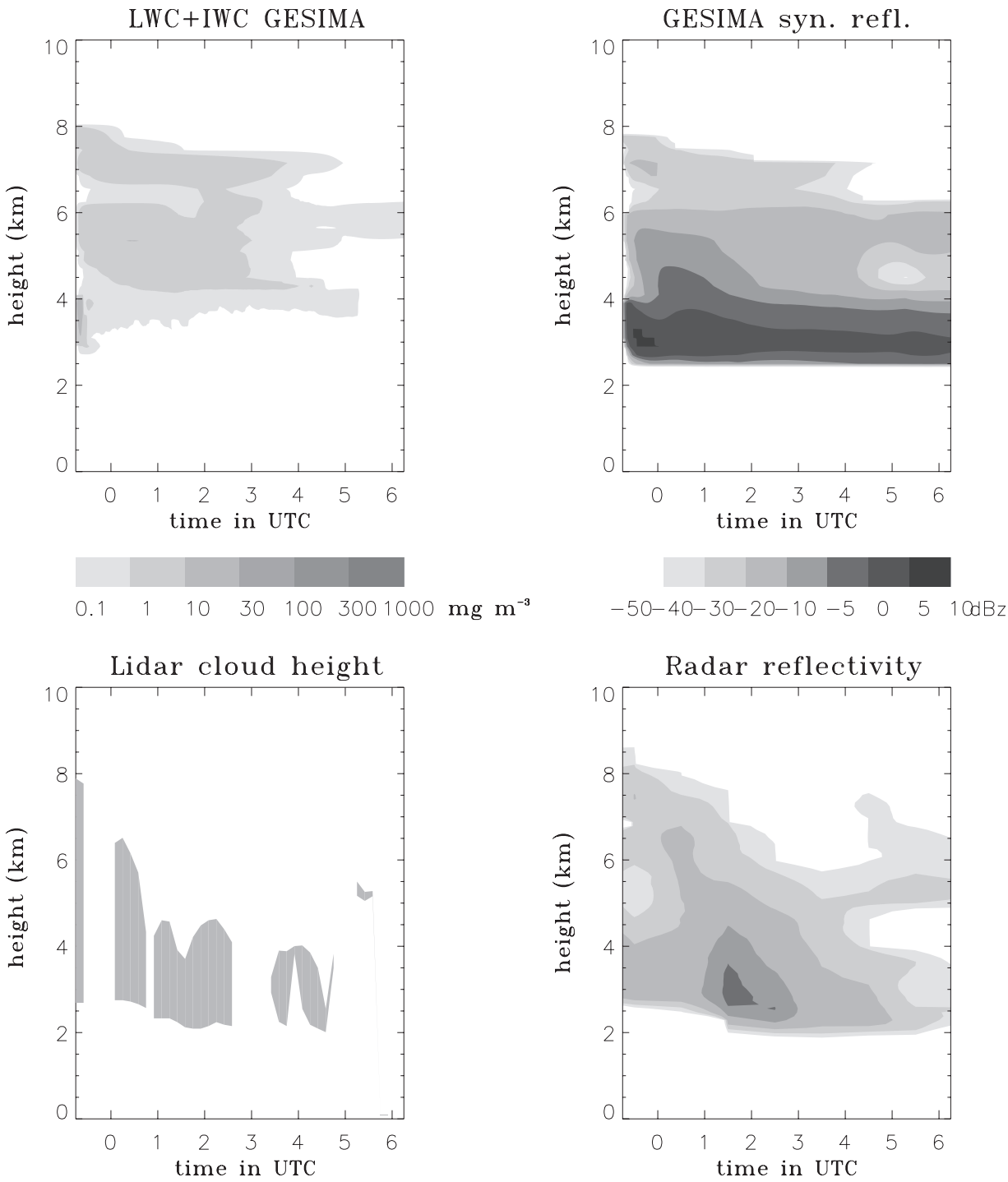

Figure 8. As in Figure 5 but for 28/29 April 1998.

However it misses the dynamical fluctuations that lead to the occasionally observed decreases of cloud base from lidar down to 2 km. Whereas the observed radar echo top decreases from 8 km at 2315 UTC to 6 km at 0300 UTC on 29 April, the simulated radar echo top lowers at a slower rate.

[33] Similar to the radar retrieval, the simulated ice crystal and snow flake effective radii and radar reflectivity increase from cloud top to cloud base and increase with time until 0130 UTC on April 29 (see Figures 8 and 9). Thereafter crystal size decreases suggestive of new ice crystal formation in the upper layer cloud and sublimation in the lower cloud. GESIMA also indicates the break up of the ice cloud in two distinct layers with a cloud free area between 4 and 5 km at 0400 UTC on 29 April in terms of ice water content, but the cloud free area is smaller and delayed by half an hour when evaluated in terms of effective ice crystal radius suggesting that the cloud has

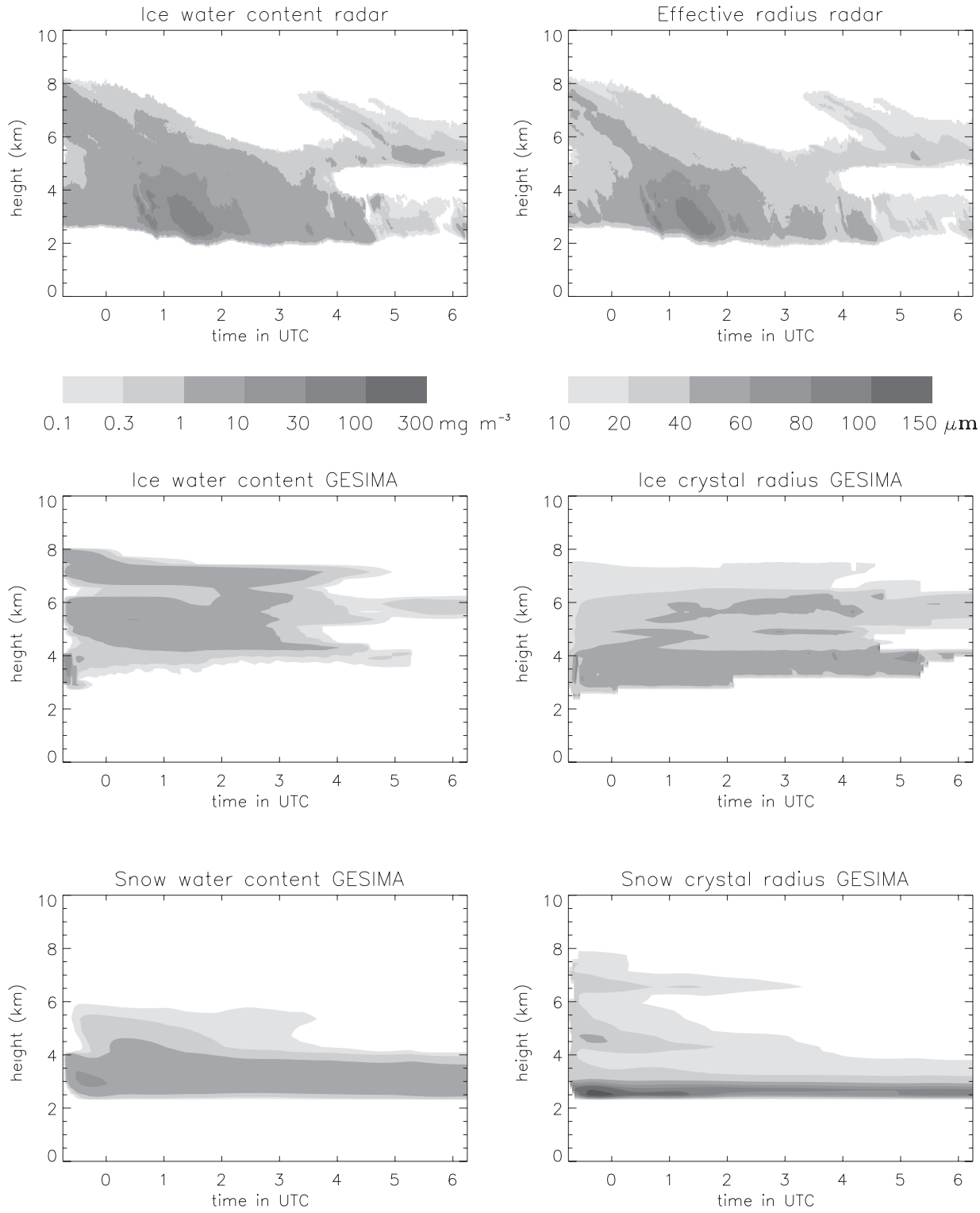

Figure 9. As in Figure 6 but for 28/29 April 1998.

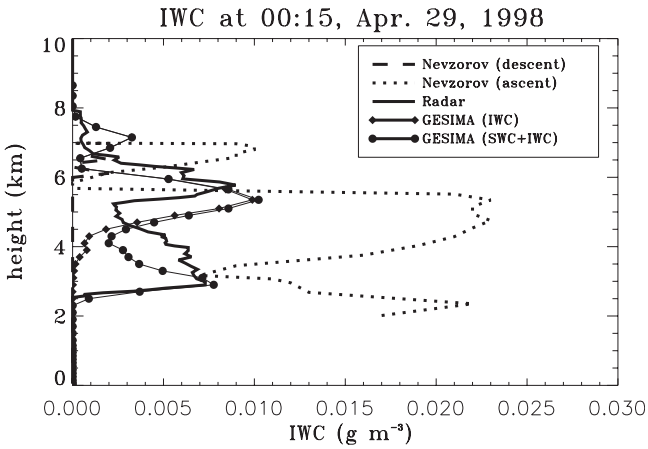

Figure 10. Vertical profiles of IWC at 0015 on 29 April 1998 simulated by GESIMA and measured by aircraft and radar retrieval.

not completely sublimated by 0400 UTC on 29 April. Moreover, the snow water content and snow crystal radii remain rather constant at cloud base instead of sublimating or sedimenting from the cloud as in the observations. This is also reflected in the calculated synthetic reflectivity shown in Figure 8.

[34] During its descent and ascent over the SHEBA ship on 28/29 April the aircraft sampled clouds. Figure 10 shows that during its descent, the Nevzorov probe measured a small IWC between 6 km and 7.2 km, whereas it sampled three cloud layers during the aircrafts ascent with peak values of IWC of 0.022, 0.023 and 0.01 g m^{-3} centered around 2 km, 5 km and 7 km. The radar retrieval shows a maximum IWC of 0.009 g m^{-3} at 6 km embedded in an ice cloud extending from 2.5 to 8 km. The simulated ice and snow water content profile has three peaks centered at 3 km, 5 km and 7 km. It is comparable in magnitude to the observed ice water content above 5 km altitude. However, the simulated cloud contains less ice than the in-situ measurements during the aircraft ascent below 5 km but it agrees well with the radar everywhere. The cloud on 28/29 April is nonprecipitating both in the observation and in GESIMA.

5. Effect of Increased Aerosol Concentrations on Precipitation

[35] In order to investigate the aerosol effect on the snowfall rate, we conduct two sensitivity experiments for the 16 April case study that only differ in their aerosol number concentrations. For the clean case, we assume a vertically uniform accumulation mode aerosol number concentration of 100 cm^{-3} (AP100) and for the polluted case we assumed 1000 cm^{-3} (AP1000). The 100 cm^{-3} case is representative of a clean atmosphere [*Peng et al.*, 2002] and was observed in the lowest levels on 16 April (Figure 11). The 1000 cm^{-3} is representative of a pollution episode [*Peng et al.*, 2002] as observed at 650 m and around 4 km during the 16 April case study (Figure 11). Even though this is an idealized experiment, it isolates the changes caused by the aerosol. If one used two different observed case studies, changes due to different weather conditions and dynamics would overwhelm the aerosol induced effects.

[36] As displayed in Figure 12, the tenfold increase in aerosol concentration leads up to an eightfold increase in the number of cloud droplets. It does not influence the upper level ice cloud, as ice crystal formation in GESIMA does not depend on the aerosol number concentration. The clean cloud is slightly thicker after 2030 UTC and does not break into two layers as the polluted cloud.

[37] As shown in Figure 13 the ice water path evolution is very similar in all simulations. Slight differences are caused by different nucleation freezing rates in AP100 and AP1000. The larger droplets in AP100 are more readily subject to immersion freezing while the more abundant droplets in AP1000 experience more contact freezing (see Figure 14).

[38] The liquid and snow water paths start to deviate after half an hour. Contrary to what one would expect from the more numerous cloud droplets in AP1000, the liquid water path is roughly twice as large in AP100 as compared to AP1000 regardless of the snow crystal shape (Figure 13 and Table 1). At the same time, the snow water path in AP100 is less than half of that in AP1000 for both aggregates and planar crystals. The built-up of cloud water in AP100 is caused by the reduced accretion of cloud droplets by snow crystals causing the lower snow water content (Figures 14 and 15). Thus, while the snow crystals are smaller above 1 km in AP1000, they are larger below

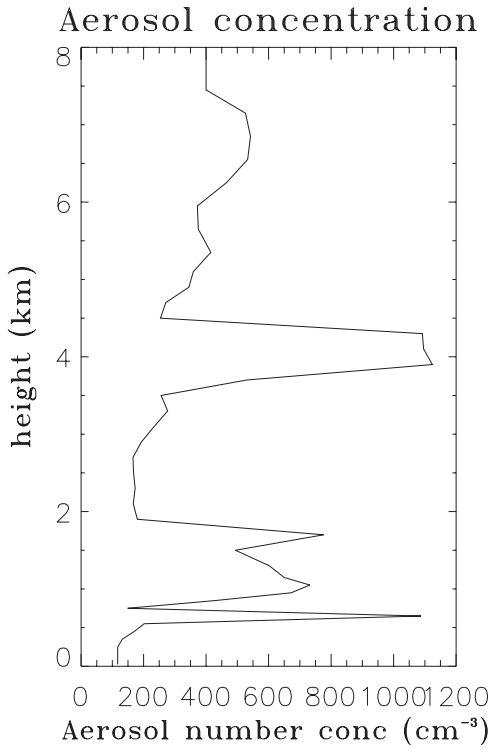

Figure 11. Vertical profile of the aerosol number concentration (cm^{-3}) from aircraft measurements on 16 April 1998.

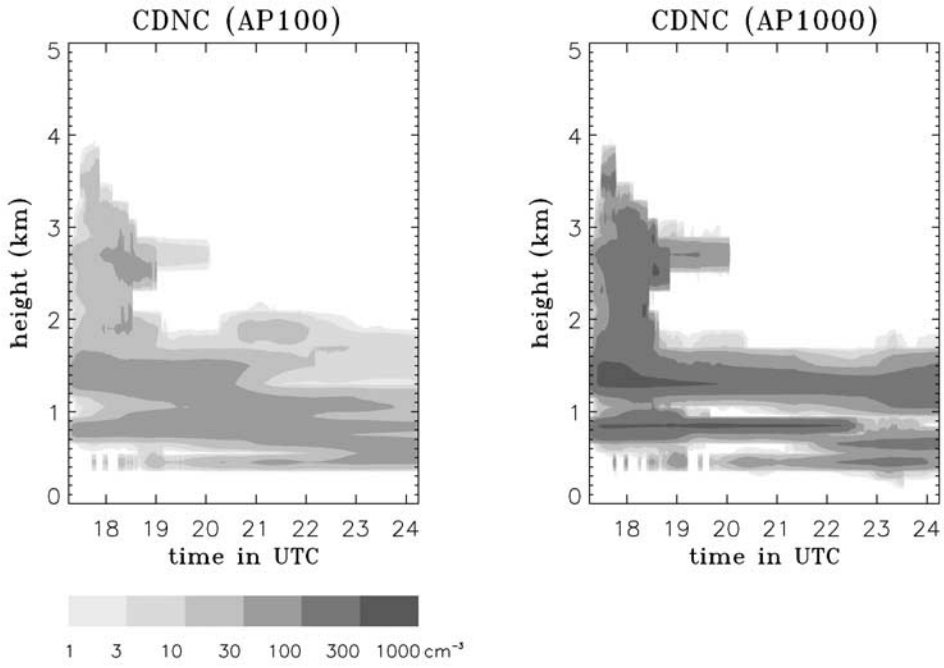

Figure 12. Temporal evolution of CDNC in the AP100 and AP1000 aerosol scenarios assuming aggregates.

1 km caused by the enhanced accretion of snow flakes with cloud droplets.

[39] The autoconversion rate which depends on the droplet radius, or for the same liquid water content is inversely proportional to the cloud droplet number concentration, is greater for the clean aerosol case compared to the continental case. Thus more liquid water is converted to drizzle in AP100 as evident after 2000 UTC. The formation of drizzle size drops then enhances their collision with snow flakes that leads to the built-up of snow water path after 2100 UTC and to increased surface precipitation as rain and snow (Figure 13).

[40] Figure 14 also shows that the accretion of drizzle by snow is significantly larger in AP100, while snow accretes more cloud droplets in AP1000. The net effect of these tendencies leads to an overall higher snow water path in AP1000 as shown in Figure 13. It takes, however, until 2300 UTC before significant amounts of surface precipitation in the form of snow appear in AP1000. The snowfall rate in AP100 exceeds that in AP1000 prior to 2345 UTC in case of aggregates at which time it overtakes in AP1000. At the end of the simulation the snowfall rate is 40% larger than in AP100. However, the snow fall rate in AP100 in case of planar crystals remains larger than in AP1000 throughout the simulation amounting to 30% accumulated over 7 hours. This is caused by the smaller collection efficiency in the polluted cloud for planar crystals as evident by the larger liquid water path and smaller snow water path as compared to the simulation assuming aggregates (Figure 13 and Table 1). The total amount of precipitation in AP100 exceeds that in AP1000 by 7% if snow crystals are aggregates and 50% in case of planar crystals. This shows that the transport of anthropogenic aerosol from Eurasia and North America to the Arctic could potentially alter snow fall rates.

6. Summary and Conclusions

[41] In this study we used the mesoscale model GESIMA to simulate Arctic mixed phase and ice clouds. We showed that for both case studies on 16 April and on 28/29 April, the simulated cloud base and top agree reasonably well with the lidar/radar retrieval. Similar to the radar retrieval, the simulated effective radii and condensed water contents decrease with height above cloud base. The simulated liquid and ice water content have the same magnitude as compared to the radar retrieval and to the observed in-situ data, but the simulated peak values occur at different altitudes.

[42] We conducted two idealized sensitivity simulations using a clean and a polluted aerosol (AP100 and AP1000, respectively) to study the effect of pollution on the Arctic precipitation. These aerosol scenario simulations suggest that Arctic clouds may be vulnerable to anthropogenic aerosols. The anthropogenic aerosols transported from Eurasia and North American result in larger cloud droplet number concentrations of cloud droplets with smaller size. While *Borys et al.* [2000] hypothesized this could decrease the snowfall rate due to the decrease in riming efficiency, we found that, on the contrary, snow accretes more cloud droplets in the polluted case. However, the more important effect is a significantly reduced accretion rate of snow crystals by drizzle size drops in the polluted cloud because of a shutdown of the collision-coalescence process. The net effect of the increase in aerosol concentration from 100 to 1000 particles cm^{-3} thus is a reduced

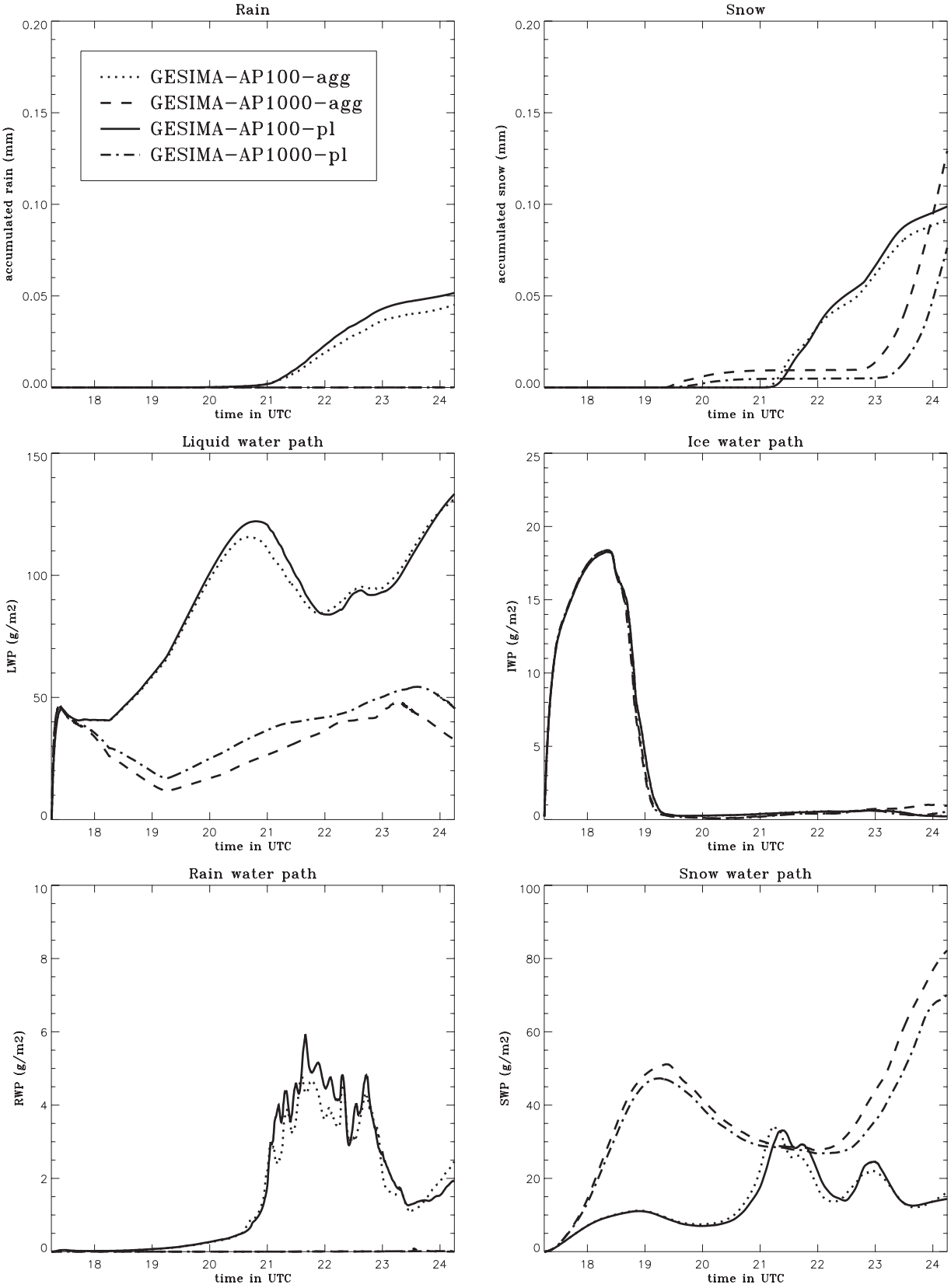

Figure 13. Temporal evolution of precipitation and liquid, ice, drizzle and snow water paths in GESIMA-CTL and AP100 and AP1000 on 16 April 1998 for the simulations assuming aggregates and planar crystals.

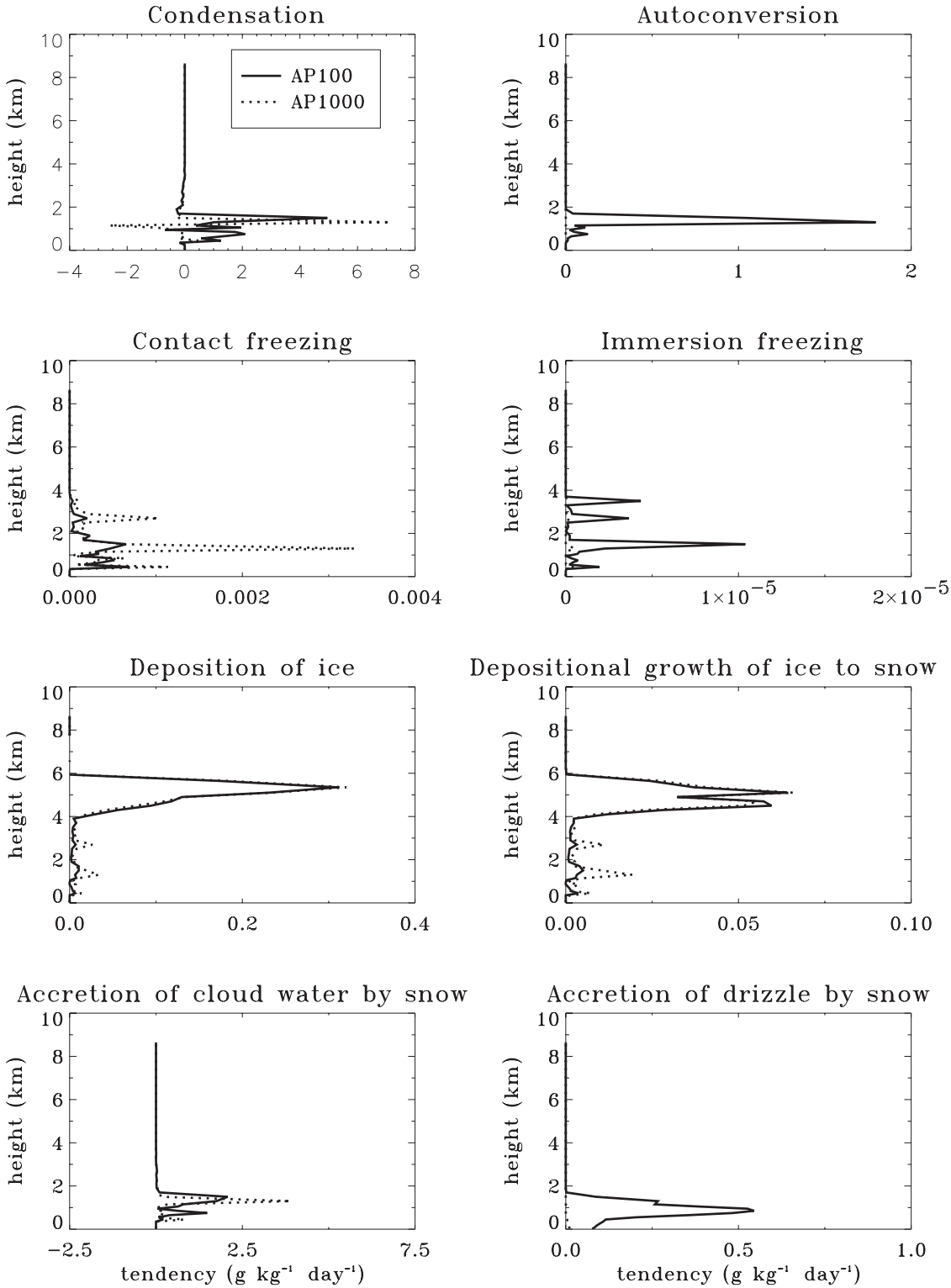

Figure 14. Vertical profiles of domain and temporal averaged cloud microphysical processes in AP100 and AP1000 assuming aggregates.

Table 1. Domain Averaged Accumulated Rain and Snow and the Domain- and Time-Averaged Liquid Water Path (LWP), Ice Water Path (IWP), Drizzle Water Path (DWP), and Snow Water Path (SWP)

	Rain, mm	Snow, mm	LWP, g m^{-2}	IWP, g m^{-2}	DWP, g m^{-2}	SWP, g m^{-2}
			Planar			
CTL	0.001	0.171	47.6	3.8	0.0	31.2
AP100	0.052	0.099	86.0	3.8	1.6	13.7
AP1000	0	0.076	36.8	3.7	0.0	34.0
AP100-AP1000	0.052	0.023	49.2	0.1	1.6	−20.3
			Aggregates			
CTL	0	0.135	37.9	3.9	0.0	28.2
AP100	0.045	0.092	84.8	3.9	1.5	13.7
AP1000	0	0.129	30.2	3.8	0.0	37.5
AP100-AP1000	0.045	−0.037	54.5	0.1	1.5	−23.9

overall surface precipitation rate in the polluted case, the magnitude of which crucially depends on the shape of the snow flakes. For aggregates it amounts to 7% while it is 50% for planar crystals. More interestingly the amount of precipitation reaching the surface as snow can be larger or smaller in AP1000 depending on the snow crystal shape. While 40% more snow reaches the surface in AP1000 after 7 hours if aggregates are assumed it is 30% less in case of planar crystals due to a smaller accretion efficiency between snow flakes and cloud droplets in the latter case.

[43] The observations by *Borys et al.* [2000] go beyond the effect of anthropogenic aerosols on warm phase precipitation, what is referred to as the cloud lifetime effect [*Albrecht*, 1989], to an effect on ice clouds by decreasing riming efficiency. Here we found that an increase in aerosol concentration decreases the overall amount of precipitation by producing less drizzle size drops necessary for accretion with snow flakes. These effects on mixed-phase cloud

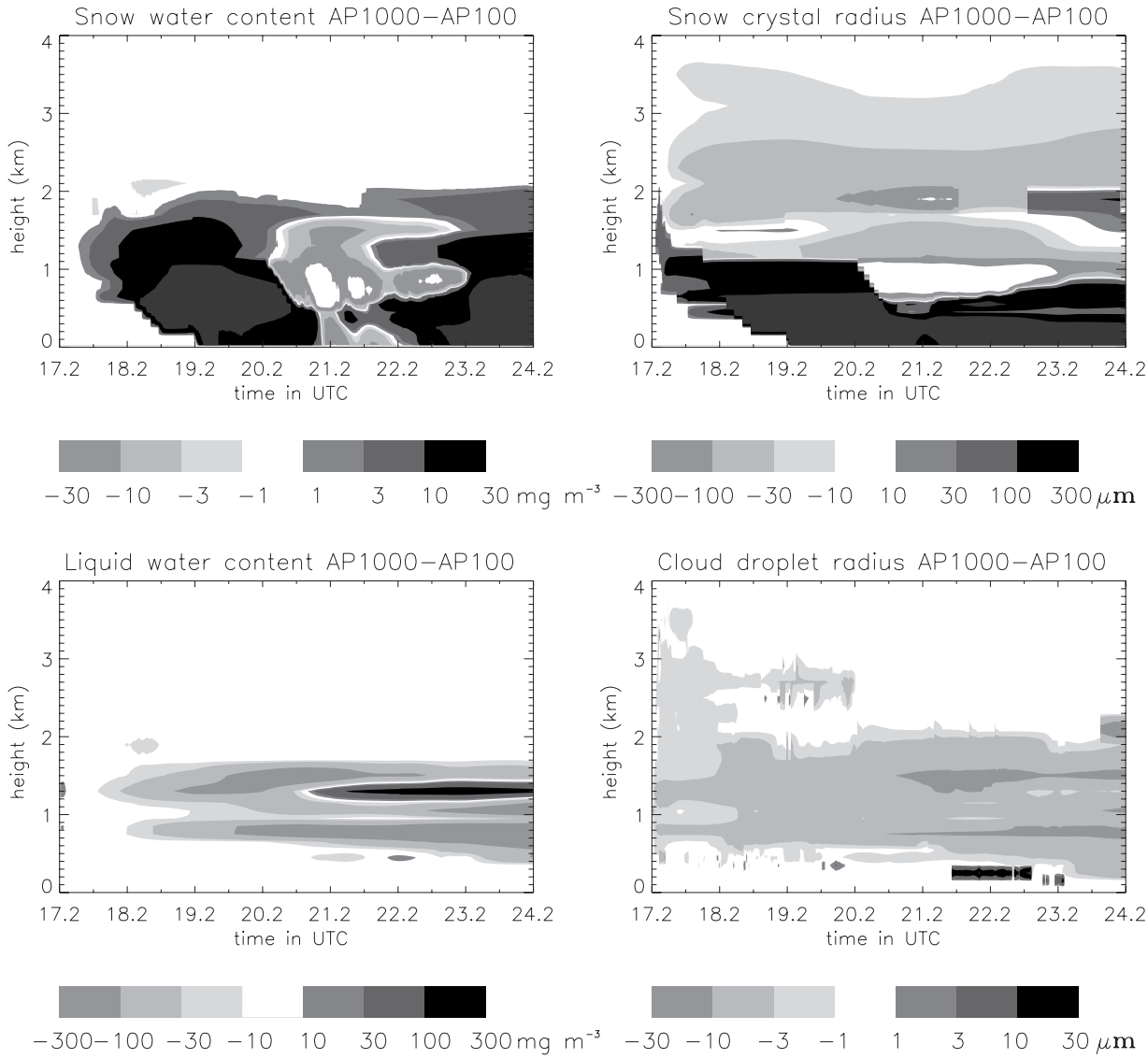

Figure 15. Vertical profiles of the differences in domain averaged snow water content, liquid water content, snow crystal size, and cloud droplet size between AP1000 and AP100 assuming aggregates.

processes can have far reaching implications since most midlatitude precipitation originates via the ice phase. However, more observations are needed in order to establish the importance of these mechanisms in different parts of the world.

[44] **Acknowledgments.** The authors thank Stewart Cober, who kindly provided the Canadian Convair-580 aircraft observational data. The radar data set was supplied by Taneil Uttal, Matthew Shupe. Richard Moritz provided corrected relative humidity data for these flights. We thank David Mitchell, Burkhardt Rockel and Glen Lesins for comments and suggestions. This research is supported by the Modeling of Clouds and Climate (MOC2) project funded by National Science and Research Council of Canada (NSERC), the Canadian Foundation for Climate and Atmospheric Science (CFCAS), the Science Subvention program of the Meteorological Service of Canada, and the NSF SHEBA project.

References

Albrecht, B., Aerosols, cloud microphysics, and fractional cloudiness, *Science*, *245*, 1227–1230, 1989.

Barrie, L. A., Occurrence and trends of pollution in the arctic troposphere, in *Chemical Exchange Between the Atmosphere and Polar Snow*, *NATO ASI Ser.*, *Ser. I*, vol. 43, edited by E. W. Wolff and R. C. Bales, pp. 93–130, Springer-Verlag, New York, 1996.

Berry, E. H., and R. L. Reinhardt, Modeling of condensation and collection within clouds, *D. R. I. Phys. Sci. Publ. 16*, Univ. of Nev., Reno, 1973.

Borys, R., D. H. Lowenthal, and D. L. Mitchell, The relationships among cloud microphysics, chemistry, and precipitation rate in cold mountain clouds, *Atmos. Environ.*, *34*, 2593–2602, 2000.

Cober, S. G., G. A. Isaac, A. V. Korolev, and J. W. Strapp, Assessing cloud-phase conditions, *J Appl. Meteorol.*, *40*, 1967–1983, 2001.

Curry, J., On the formation of continental polar air, *J. Atmos. Sci.*, *40*, 2279–2292, 1983.

Curry, J. A., W. B. Rossow, D. Randall, and J. Schramm, Overview of arctic cloud and radiation characteristics, *J. Clim.*, *9*, 1731–1764, 1996.

Curry, J. A., et al., Fire arctic cloud experiment, *Bull. Am. Meteorol. Soc.*, *81*, 5–30, 2000.

Ghan, S. J., C. C. Chuang, and J. E. Penner, A parameterization of cloud droplet nucleation, part I, Single aerosol type, *Atmos. Res.*, *30*, 197–221, 1993.

Girard, E., and J.-P. Blanchet, Simulation of arctic diamond dust, ice fog, and thin stratus using an explicit aerosol-cloud-radiation model, *J. Atmos. Sci.*, *58*, 1199–1221, 2001.

Gorshkov, S., *World Ocean Atlas*, vol. 3, *The Arctic Ocean*, Pergamon, New York, 1983.

Houghton, J. T., Y. Ding, D. J. Griggs, M. Noguer, P. J. van der Linden, X. Dai, K. Maskell, and C. A. Johnson (Eds.), *Climate Change 2001: The Scientific Basis, Contribution of Working Group I to the Third Assessment Report of the Intergovernmental Panel on Climate Change*, Cambridge Univ. Press, New York, 2001.

Huschke, R., Arctic cloud statistics from "air-calibrated" surface weather observations, *RM6173-PR*, Rand Corp., Santa Monica, Calif., 1969.

Jiang, H., W. R. Cotton, J. O. Pinto, J. A. Curry, and M. J. Weissbluth, Cloud resolving simulations of mixed-phase arctic stratus observed during BASE: Sensitivity to concentration of ice crystals and large-scale heat and moisture advection, *J. Atmos. Sci.*, *57*, 2105–2117, 2000.

Kapitza, H., and D. Eppel, The non-hydrostatic mesoscale model GESIMA, part I: Dynamical equations and tests, *Contrib. Atmos. Phys.*, *65*, 129–145, 1992.

Khairoutdinov, M., and Y. Kogan, A new cloud physics parameterization in a large-eddy simulation model of marine stratocumulus, *Mon. Weather Rev.*, *128*, 229–243, 2000.

Korolev, A. V., G. A. Isaac, and J. Hallett, Ice particle habits in Arctic clouds, *Geophys. Res. Lett.*, *26*, 1299–1302, 1999.

Levkov, L., B. Rockel, H. Kapitza, and E. Raschke, 3D mesoscale numerical studies of cirrus and stratus clouds by their time and space evolution, *Contrib. Atmos. Phys.*, *65*, 35–58, 1992.

Lew, J. K., D. C. Montague, and H. R. Pruppacher, A wind tunnel investigation on the riming of snowflakes, part I: Porous disks and large stellars, *J. Atmos. Sci.*, *43*, 2392–2409, 1986.

Lin, B., P. Minnis, A. Fan, J. A. Curry, and H. Gerber, Comparison of cloud liquid water paths derived from in situ and microwave radiometer data taken during the SHEBA/FIREACE, *Geophys. Res. Lett.*, *28*, 975–978, 2001.

Lin, Y. L., R. D. Farley, and H. D. Orville, Bulk parameterization of the snow field in a cloud model, *J. Clim. Appl. Meteorol.*, *22*, 1065–1092, 1983.

Lohmann, U., J. Feichter, C. C. Chuang, and J. E. Penner, Predicting the number of cloud droplets in the ECHAM GCM, *J. Geophys. Res.*, *104*, 9169–9198, 1999.

Lohmann, U., J. Humble, W. R. Leaitch, G. A. Isaac, and I. Gultepe, Simulations of ice clouds during FIRE ACE using the CCCMA single column model, *J. Geophys. Res.*, *106*, 15,123–15,138, 2001.

Matrosov, S. Y., Variability of microphysical parameters in high-altitude ice clouds: Results of the remote sensing method, *J. Appl. Met.*, *36*, 633–648, 1997.

Mellor, G. L., and T. Yamada, Development of a turbulence closure model for geophysical fluid problems, *Rev. Geophys.*, *20*, 851–875, 1974.

Meyers, M. P., P. J. DeMott, and W. R. Cotton, New primary ice-nucleation parameterization in an explicit cloud model, *J. Appl. Meteorol.*, *31*, 708–721, 1992.

Mitchell, D. L., Evolution of snow-size spectra predicted by the growth processes of diffusion, aggregation and timing, paper presented at Conference on Cloud Physics, Am. Meteorol. Soc., San Francisco, Calif., 1990.

Peng, Y., U. Lohmann, R. Leaitch, C. Banic, and M. Couture, The cloud albedo-cloud droplet effective radius relationship for clean and polluted clouds from RACE and FIRE, ACE, *J. Geophys. Res.*, *107*(D11), 4106, doi:10.1029/2000JD000281, 2002.

Pruppacher, H. R., and J. D. Klett, *Microphysics of Clouds and Precipitation*, Kluwer Acad., Norwell, Mass., 1997.

Rogers, R. R., and M. K. Yau, *A Short Course in Cloud Physics*, Pergamon, New York, 1989.

Schweiger, J., and J. Key, Artic cloudiness: Comparison of ISCCP-C2 and Nimbus-7 satellite-derived cloud products with a surface-based cloud climatology, *J. Clim.*, *5*, 1514–1527, 1992.

Shupe, M., T. Uttal, S. Y. Matrosov, and A. S. Frisch, Cloud water contents and hydrometeor sizes during the FIRE-Arctic Cloud Experiment, *J. Geophys. Res.*, *106*, 15,015–15,028, 2001.

Uttal, T., et al., Surface heat balance of the Arctic Ocean, *Bull. Am. Meteorol. Soc.*, *83*, 255–275, 2002.

Warren, S., and W. Wiscombe, A model for the spectral albedos of snow, part II: Effects of aerosols, *J. Atmos. Sci.*, *37*, 2734–2750, 1980.

Wood, R., Drizzle in stratocumulus: Observations and model results, paper presented at 11th AMS Conference on Cloud Physics, Am. Meteorol. Soc., Ogden, Utah, 2002.

Zhang, J., and U. Lohmann, Sensitivity of single column model simulations of Arctic springtime clouds to different cloud cover and mixed phase cloud parameterizations, *J. Geophys. Res.*, *108*, doi:10.1029/2002JD003136, in press, 2003.

U. Lohmann and J. Zhang, Department of Physics and Atmospheric Science, Dalhousie University, Halifax, Nova Scotia, Canada B3H 3J5. (ulrike.lohmann@dal.ca)

J. Pi, Computer Science Department, University of Nebraska at Omaha, Omaha, NE 68182, USA.